Nonlinear optical effects in a two-dimensional photonic crystal containing one-dimensional Kerr defects

M. Bahl,[1,*] N.-C. Panoiu,[2] and R. M. Osgood, Jr.[1,3]
[1]*Department of Electrical Engineering, Columbia University, New York, New York 10027*
[2]*Department of Applied Physics and Applied Mathematics, Columbia University, New York, New York 10027*
[3]*Brookhaven National Laboratories, Upton, New York 11973*
(Received 11 December 2002; revised manuscript received 12 February 2003; published 9 May 2003)

The nonlinear optical effects induced by a one-dimensional (1D) line defect, made of Kerr material, in a 2D photonic crystal are studied. Comprehensive *ab initio* numerical simulations based on the finite-difference time-domain method show efficient third-harmonic generation in a photonic crystal waveguide consisting of the 1D defect line. The relationship between the third harmonic generation process and the nonlinear modal properties of the waveguide is discussed. We investigate optical limiting in such a device, that is, control of the transmitted power as a function of the Kerr-induced variation of the refractive index. Power dependent spectral changes in such a device and its use as a frequency selector are also examined.

DOI: 10.1103/PhysRevE.67.056604 PACS number(s): 42.65.Wi, 42.65.Ky, 42.79.−e, 42.25.Bs

I. INTRODUCTION

During the last decade the physical properties of photonic crystals (PCs) have been a fruitful research area. PCs are dielectric structures whose spatial modulation of refractive index leads to a profound change of the photon dispersion relation [1–3]. Photonic crystals can be seen as the optical analog of semiconductors, i.e., photonic band gap (PBG) materials display gaps in their photon density of states. Furthermore, defects in their periodic structure can introduce localized states (modes) within the band gaps [4]. This analogy has helped drive research efforts to find technological applications for PBG materials. Thus, two-dimensional (2D) and (3D) PCs at optical frequencies have been fabricated over the past few years and several optical-device applications have been proposed and demonstrated. For instance, it has been demonstrated that linear defects in PBG materials can act as efficient waveguides, transmitting light around sharp corners with relatively small losses [5,6]. Furthermore, under certain circumstances, pointlike defects in PBG materials behave as resonant microcavities that can be used to efficiently couple light into PBG-based waveguides. This effect can be used to design resonant add-drop filters [7] and other integrated optical components [8–12]. Potentially, these applications can lead to the design of new compact integrated optoelectronic or all-optical circuits.

One emerging area of research in PCs is dynamical control of their optical properties. Several studies have shown that external variation of the PC refractive index can lead to changes in the band-gap structure of the material. These effects include changes in the refractive index through variation in temperature [13], the electro-optic effect [14], charge-carrier injection, or photorefraction [15]. The main drawback of all these schemes is that they are generally rather slow compared to the speeds required by modern communications systems.

One promising approach, which is suitable for ultrafast devices, is to employ intrinsic (Kerr) nonlinearities in the PC material. A Kerr material having a nonlinear refractive index leads to a nonlinear PBG, whose band structure can be controlled by the intensity of the input optical signal. Kerr-active defects can be embedded in the PC to form waveguides or resonant cavities. The enhanced driving fields present at these defects can induce effects with potential applications: efficient higher harmonic generation or switching at reduced optical energies. For instance, giant third-harmonic generation (THG) in a (1D) PC-based microcavity [16] has been recently demonstrated. Thus, it has been shown that the strong localization of the optical field near the cavity can lead to an enhanced THG efficiency; this enhanced TH intensity at the frequency of the cavity mode can be three orders of magnitude higher as compared to the intensity of the TH generated at other frequencies within the band gap. In our analysis, we focus on effects induced by a 1D nonlinear Kerr defect embedded in a 2D linear PC.

The influence of the Kerr defects inserted in a 1D PC on the transmission properties of a slab of crystal was first studied in [17] and a dynamical shift in the location of the band gap, due to the nonlinear medium response, was reported. Also, the existence of stable nonlinear localized modes (solitons) in *weakly* modulated 2D and 3D PCs, with Kerr nonlinearity, was predicted in Ref. [18]. Recently, the existence of new types of nonlinear guiding modes was reported in Refs. [19,20]. These modes are created by inserting a 1D Kerr defect in a linear 2D PC and are localized, by the defect, in a direction transverse to the waveguide axis.

In this article, we study the properties of such nonlinear modes and their applications to THG and optical limiting. Our approach avoids any approximations to the underlying governing equations, thus allowing a first-principles analysis. An exact treatment is necessary since small variations in the field can cause a major change in the optical properties of such a structure. The paper is organized as follows. In Sec. II we describe the crystal geometry and introduce the numerical method used here, i.e., the finite-difference time-domain (FDTD) method, and the modifications needed to incorporate

*Electronic address: mayank.bahl@columbia.edu

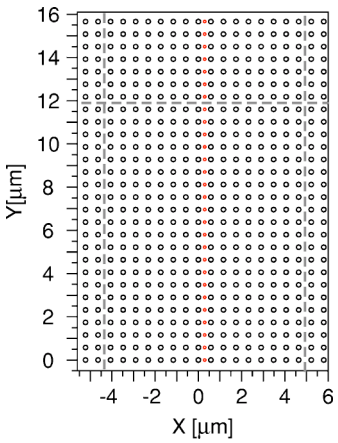

FIG. 1. A PC with a column of nonlinear defect rods. The dashed lines show the boundaries of the PC-based perfectly matched layer. The parameters of the PC are as follows: lattice constant $a=0.58$ μm, radius of the lattice rods $r=0.18a$, radius of the defect rods $r_d=0.1a$, and dielectric constant of the lattice rods and linear part of the dielectric constant of the defect rods $\epsilon_l=11.56$.

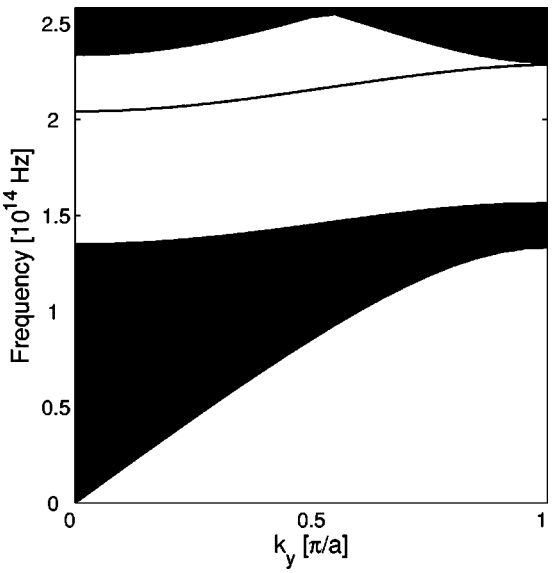

FIG. 2. The localized defect mode (solid line) within the photonic band gap for our photonic crystal with a line defect. The parameters of the photonic crystal are those in Fig. 1.

nonlinear materials. In Sec. III, we discuss the characteristics of THG by the 1D nonlinear line defect. In the subsequent section, we analyze the power limiting behavior induced by such nonlinear modes. In this same section we also discuss the tunability and frequency selectivity of potential devices that exploit the properties of these nonlinear modes. Finally, we conclude with a summary and discussion of our results.

II. NUMERICAL APPROACH

Our numerical simulations use a 2D rather than a 3D geometry for the PC. This reduces the computation time considerably, while still capturing the essential physics of the problem. We consider a lattice of rods, with 55 rows and 20 columns, made from a linear optical material having a column of Kerr-active defect rods. The z axis is aligned with the rods. The electric field is polarized along this axis (TM polarization) and propagates in the (x,y) plane.

The geometry of the PC and its dimensions are presented in Fig. 1. Its dimensions and linear dielectric constant $\epsilon_l=11.56$ were chosen such that the first band gap is centered at $\lambda=1.55$ μm. As Fig. 2 illustrates, by inserting a line defect made from *linear* material into the photonic crystal, a guiding defect mode is formed within the first band gap. The band diagram of Fig. 2 is constructed using only the linear optical properties of the crystal and assumes an infinite crystal. The minimum guiding frequency is $\omega_c=1.282\times10^{15}$ Hz and corresponds to the center of the Brillouin zone, $k=0$, whereas the maximum frequency is $\omega_b=1.437\times10^{15}$ Hz and corresponds to the boundary of the Brillouin zone, $k=\pi/a$. This gives a mode bandwidth of $\Delta\omega=1.55\times10^{14}$ Hz. For a shorter crystal, the structure of the guiding mode consists of a number of discrete crystal states or modes, usually equal to the number of Kerr rods within the line defect in the crystal. For a sufficiently short crystal, these discrete modes can be resolved in the transmission spectra. For most of this article we consider long crystals with a large number of defect rods along the longitudinal direction. Consequently, the guiding mode contains a large number of discrete states; however, its fine spectral structure is not resolved over the simulation times used in our computations. This is not a limitation of our approach but rather a simplification introduced to reduce the computational time. In fact, in the last part of Sec. IV, the discrete modal spectrum is considered in detail when the properties of a small crystal are investigated.

In order to simulate light propagation within this PC structure, we used the FDTD method [21], which solves the complete set of Maxwell's equations on a spatial grid that contains the structure of interest. Since the FDTD method is well known and widely used in many areas of computational electromagnetics (for a detailed presentation of the FDTD method, see Ref. [22]), we present here only those features concerning its application to structures containing nonlinear materials. The Kerr effect is modeled by introducing an intensity-dependent change of the refractive index:

$$\Delta n=\frac{n_2 I}{1+I/I_{sat}}, \tag{1}$$

where Δn is the change in the refractive index, I is the local intensity of light and is proportional to $|E|^2$, I_{sat} is the saturation intensity of the nonlinearity, and n_2 is proportional to the third-order nonlinear susceptibility $\chi^{(3)}$. Equation (1) can be cast in a dimensionless form,

$$\Delta n=\frac{\overline{n_2}|u|^2}{1+\alpha|u|^2}. \tag{2}$$

Here, $\overline{n_2}$ and $u(x,y)$ are the dimensionless nonlinear refractive index and the dimensionless field amplitude, respec-

tively, and α is a dimensionless coefficient. The relationship between the field intensity I and the normalized field u is

$$I=\beta|u|^2, \tag{3}$$

where the constant β is determined from the initial condition

$$P_{in}=\beta\int |u(x,0)|^2 dx. \tag{4}$$

Here, P_{in} is the total power per unit length launched into the crystal and the integral is taken along the phase front of the input field. The input field $u(x,0)$ is normalized such that the integral in Eq. (4) is equal to 1 μm. In our computations, for simplicity, we assume that the fields are much less than that required for saturation, i.e.,

$$u_{max}^2 \ll \frac{1}{\alpha}. \tag{5}$$

Thus, the change in the refractive index is simply given by

$$\Delta n=\overline{n_2}|u|^2, \tag{6}$$

where $\overline{n_2}=n_2\beta$, so that the required input parameters are the input power P_{in} and the nonlinear refractive index n_2.

In order to include optical nonlinearity into the FDTD algorithm, a nonlinear polarization term is added to the linear polarization term in Maxwell's equations. Thus, the linear polarization term is given by

$$\mathbf{P}^L=\epsilon_0\int \chi^{(1)}(t-\tau)\mathbf{E}(\mathbf{r},\tau)d\tau \tag{7}$$

and the nonlinear polarization term that models an instantaneous response of the medium is given by

$$\mathbf{P}^{NL}=\epsilon_0\chi^{(3)}|\mathbf{E}(\mathbf{r},t)|^2\mathbf{E}(\mathbf{r},t), \tag{8}$$

where $\chi^{(3)}(t)$ is the third-order susceptibility and $\mathbf{r}=(x,y)$ is the position vector. The electric field is related to the displacement vector by

$$\mathbf{E}=\frac{\mathbf{D}-\mathbf{P}^L-\mathbf{P}^{NL}}{\epsilon_0}. \tag{9}$$

The above equations, coupled with the Maxwell equations, can then be solved iteratively by using Yee's central-difference scheme to yield the field distribution over the finite grid [22]. These *nonlinear* FDTD simulations were performed using the commercially available software FULLWAVE [23].

The grid used to discretize Maxwell's equations contained $N_x=508$ points in the x direction; there were five computational points across a nonlinear rod (the smallest structures in the PC). Along the longitudinal direction y, $N_y=1620$ points. Our numerical computations showed that the fields reached a negligible value after a distance of ten rods, in a direction perpendicular to the defect line. Therefore, we were able to use a relatively small number of rods in the transverse direction.

In order to reduce reflections from the boundaries of the PC, we employed a PC-based perfectly matched layer (PML) method [24]. Thus, the PML that terminates the computational domain contains seven rows of the crystal in the longitudinal direction, and two rows on each side of and transverse to the line defect. The area containing the PML rods is delineated in Fig. 1 by a dashed line. As compared to the case when the PC is terminated simply by a standard PML, this approach reduces the reflections from the boundaries by as much as three orders of magnitude. The efficiency of this approach stems from an improved matching of the propagation constants of the modes propagating in the PC and the decaying waves in the PML. We chose to place the PML boundary at the midpoint between two rods since it is known to be the optimum location for minimum reflection from the PML [24].

Finally, the time step in the FDTD simulations is an important component of the numerical method. In linear optical materials, the smallest step is determined by the Courant stability limit [22]. However, when regions containing nonlinear materials are introduced into the computational domain, this limit is no longer valid; there is then no *a priori* criterion to determine the time step. Therefore, for a fixed set of input parameters, we reduced the time step until additional changes caused no further alteration of the computed results. In fact, in certain cases, we had to reduce the time step to one-tenth of the corresponding Courant limit.

III. HARMONIC GENERATION

Consider an optical pulse, whose central frequency is at or slightly detuned from that of the guiding mode at $\mathbf{k}=0$ and whose intensity is high enough to induce appreciable changes in the nonlinear refractive index. When such a pulse is launched into a photonic crystal, the light will be transversely confined and guided by the line defect with the waveguide properties changed from those at low input power. In addition, we will show below that Kerr-active defects can generate a third harmonic with relatively high conversion efficiency. An obvious advantage of using line defects of Kerr active materials as opposed to previously proposed schemes, e.g., pointlike Kerr defects or Kerr-active microcavities embedded in 1D line defects, is that one obtains a larger active region where the TH is generated, and, consequently, higher efficiencies.

To investigate these phenomena, we launched Gaussian pulses, in both time and space, into the photonic crystal. These pulses had a full width at half maximum of 17.6 fs, corresponding to a power spectral width of $\Delta\omega_p=9.5\times10^{13}$ Hz. This value was chosen such that the spectral bandwidth of the pulses fit within the band gap and the entire range of frequencies in the guiding mode is covered. An increase in the pulse bandwidth, such that a part of the pulse lies in the continuum band, would inject unwanted radiation into the PC and is thus avoided. In contrast, a pulse with a smaller bandwidth would have a smaller frequency overlap with the guiding mode, so that a lesser amount of radiation would be coupled into the crystal. Therefore, in this respect, the pulse bandwidth we chose was optimal for our numerical

investigations. The center frequency of the pulse, $\omega_0 = 1.263 \times 10^{15}$ Hz, is slightly detuned from the defect mode frequency at $k=0$, ω_c. The input pulse was focused to a spot having a $1/e$ width of the lattice period a at a point situated at $0.7a$ from the input facet of the crystal. We varied both the power of the input pulse and the nonlinear refractive index of the defect rods.

Since the FDTD method completely describes the dynamics of the full electromagnetic field, no approximations are made when this method is employed. To be more specific, we avoid the approximations that are usually made in the slowly varying amplitude formalism. As a consequence, the influence of effects such as self-phase modulation, cross-phase modulation, or four-wave mixing on the higher harmonic generation process are treated in a unitary manner. Furthermore, our FDTD-based numerical simulations show that the electric field varies significantly across the defect rods, an effect which has not always been considered in some earlier studies [20]. For example, our computation shows that the variation of the field between two grid points within the defect rods can be as high as 20%. Therefore, in these situations, one cannot apply the effective discrete equation model introduced recently in Ref. [25], since it assumes that the fields across the defect rods are constant. Moreover, since the defect rods are closely spaced, one cannot use the coupled-resonator optical waveguide (CROW) approach [26,27], a powerful method that can provide analytic results but that is accurate only when the distance between the defect rods is rather large, such that the defect modes associated with these defect rods are weakly coupled.

The efficiency of the THG process was determined by computing the fields at a series of distances from the source along the waveguide. These field data were then Fourier transformed and squared to obtain the power spectral density (PSD). The power at the TH and the fundamental is then calculated by integrating the PSD in the frequency domain around ω_0 and $3\omega_0$, respectively. The power at the TH is then normalized to the power at the fundamental. A typical example of the spectral output is shown in Fig. 3(a). It shows that a degenerate four-wave mixing process, viz., THG, yields a pulse at $3\omega_0$.

Figure 3(b) shows the efficiency of the conversion process as a function of distance along the waveguide for three different Kerr coefficients. The field increases at the input facet and then peaks before attaining an almost constant value, which then slowly decreases over the remaining length of the crystal. The initial transient phase in Fig. 3(b) is due, in part, to the optical clamping phenomena of the fundamental; this will be discussed in the next section. The conversion efficiency, which can be calculated from the data in Fig. 3(b), is significant. For example, the THG efficiency calculated this way is 1% for $n_2 = 1\ \mu\text{m}^2/\text{W}$ and an input power of $1\ \text{W}/\mu\text{m}$. The relatively high conversion efficiency is due, in part, to the tight lateral confinement of the fundamental in the defect line.

The data in Fig. 3(b) also show that there is a clear optimum in the THG efficiency. In particular, Fig. 3(b) shows that the THG efficiency is sensitive to the variation of the Kerr coefficient of the defect rods. Two competing factors

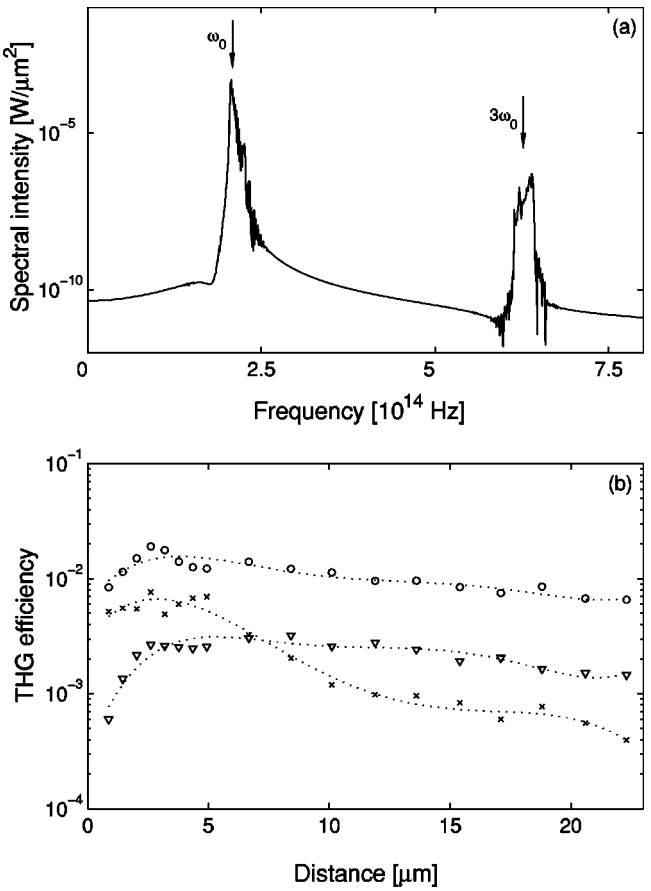

FIG. 3. (a) The output spectral density of the optical field for $n_2 = 0.1\ \mu\text{m}^2/\text{W}$ and $P_{in} = 1\ \text{W}/\mu\text{m}$. (b) The ratio of the peak intensity of the third harmonic and the fundamental wave vs propagation distance for $n_2 = 1\ \mu\text{m}^2/\text{W}$ (○), $n_2 = 0.1\ \mu\text{m}^2/\text{W}$ (▽), and $n_2 = 5\ \mu\text{m}^2/\text{W}$ (×). The input power, in all cases, was $P_{in} = 1\ \text{W}/\mu\text{m}$.

determine the value of n_2 for which the conversion efficiency is highest. First, at low values of n_2, increasing the Kerr coefficient of the defect rods enhances the nonlinear conversion process, thus increasing the generated TH. On the other hand, for large Kerr nonlinearities, as we show in the next section, the transmitted power sharply decreases with the increase of the input power, which, in turn, decreases the THG efficiency.

A spatial mapping of the TH field shows that it is confined in the transverse direction. This apparent confinement occurs despite the fact that the frequency of the TH is within the continuum of the PC. This shows that the rate of THG at the defect rods is far greater than the rate at which it diffracts through the crystal and therefore the TH appears spatially confined. To analyze the degree of this apparent confinement, the generated TH was monitored at several locations in the transverse direction, after the pulse had propagated eight rows along the longitudinal direction. The first monitor point was located at the defect rod while the remaining points were at the first three periods from the defect line, on both sides in the transverse direction. Then, as before, we determined the PSD of the fields at these monitoring points and the power in the TH was calculated. The results are shown in Fig. 4. The

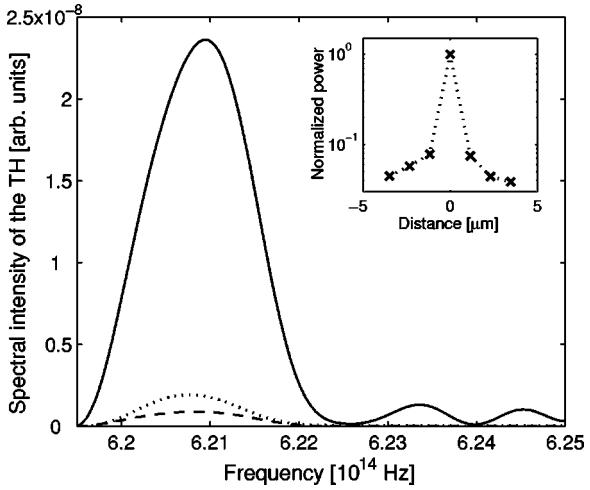

FIG. 4. The spectral density of the optical field at three transverse positions with respect to the line defect: at the defect line (continuous line), one period from the defect line (dotted line), and two periods from the defect line (dashed line). In the inset, the normalized power of the TH vs the transverse distance.

power in the TH at the first three periods, normalized to the power of the TH at the defect line, is presented in the inset. As this figure illustrates, the TH is strongly confined along the transverse direction, almost vanishing after a few lattice constants. Similar calculations, for other propagation distances, show that the TH remains confined near the defect line. This characteristic of the THG process renders it useful for potential applications in integrated frequency convertors.

Interestingly, the group velocity associated with the dispersion curve of the guiding mode shown in Fig. 2, given by $v_g = \partial\omega/\partial k$, is extremely small, especially near the edge and the center of the Brillouin zone. This was observed by recording the time required for a pulse to cross a particular monitoring point. Since the power flux P of the propagating mode is directly proportional to the product of the group velocity and the field intensity, the field intensity within the crystal will be enhanced over that in free space, for the same power flux. For example, for $n_2 = 1\ \mu\text{m}^2/\text{W}$ and an input power of 1 W/μm the field intensity is approximately ten times that at the input facet of the crystal. This strong enhancement of the optical field leads to high harmonic conversion.

Figure 3(b) shows that the efficiency of the THG is strongly dependent on the nonlinear refractive index n_2, and, implicitly, on the power in the defect mode. Other factors also determine the efficiency of the THG. For example, due to the fact that the shape and position of the defect mode in the band gap affect the degree of confinement of the field near ω_0 and the amount of power that is coupled into the crystal, the parameters of the defect line will also influence the efficiency of the THG process. Also, as will be clear from the results in the next section, the input power plays an important role in setting the transmission properties of the crystal in the defect region and, consequently, the efficiency of the THG process.

IV. OPTICAL LIMITING AND FREQUENCY SELECTION

One interesting potential application of nonlinear photonic crystals is that of optical limiting. In the version of the device studied here, a change in the index of the material, caused by the input pulse, shifts the frequency spectrum of the propagating defect mode, thus modifying the device transmission. The process will be controlled by the nonlinear Kerr coefficient n_2 and by the input power P_{in}. Since in an experimental setup n_2 and P_{in} are free parameters, we studied the influence of these two parameters on the characteristics of the optical limiting process.

Optical limiting was studied by first launching pulses into the crystal while varying the input power. In addition, limiting was also examined for different choices of Kerr coefficients, with a fixed input power. Our crystal geometry was chosen such that, at the frequency of the defect mode, the crystal is essentially transparent for very low input powers. Figures 5(a)–5(c) show the transverse spatial distribution of $|E|^2$ for an input peak pulse power of $P_{in} = 1$ W/μm at three different propagation times, or distances along the defect line. As is shown in the figure, at the end of the crystal the transmitted intensity has decreased to less than one-half of the input intensity. Limiting is even more evident in Figs. 5(d)–5(f) which show the same intensity distribution for an input power of $P_{in} = 10$ W/μm. In this case, the intensity of the transmitted pulse at the output is more than two orders of magnitude smaller than the input intensity.

One factor that determines this behavior is the frequency shift of the guiding mode, induced by the change in the refractive index. Thus, as the mode is shifted in frequency, the overlap between the bandwidth of the mode and the bandwidth of the pulse changes, leading to a variation of the amount of power coupled into the crystal. The frequency shift $\delta\omega(k)$, at a particular k, can be evaluated by using perturbation theory; the result is

$$\delta\omega(k) = -\kappa \frac{\omega(k)\,\delta n}{n}, \tag{10}$$

where κ is the ratio between the energy of the mode contained in the regions where $\delta n \neq 0$ and the total energy of the mode. This equation shows that for self-focusing materials ($n_2 > 0$) the mode is shifted to lower frequencies. Equation (10) can be used to calculate the change in the refractive index of the small rods, Δn_{cr}, required to shift the highest guiding frequency ω_b to frequencies lower than that of the input; this would give an estimation for the change in the refractive index required for the extinction of the transmitted power. However, since the field distribution corresponding to a particular mode cannot be determined rigorously when the PC contains nonlinear material, we chose another method to calculate Δn_{cr}: we determined the band structure of the PC for increasing values of the refractive index of the small rods, and found the value of the refractive index change at which the threshold condition described above is met. The result is $\Delta n_{cr} \approx 1.3$. This value is smaller than the change of the refractive index in the case presented in Figs. 5(d)–5(f),

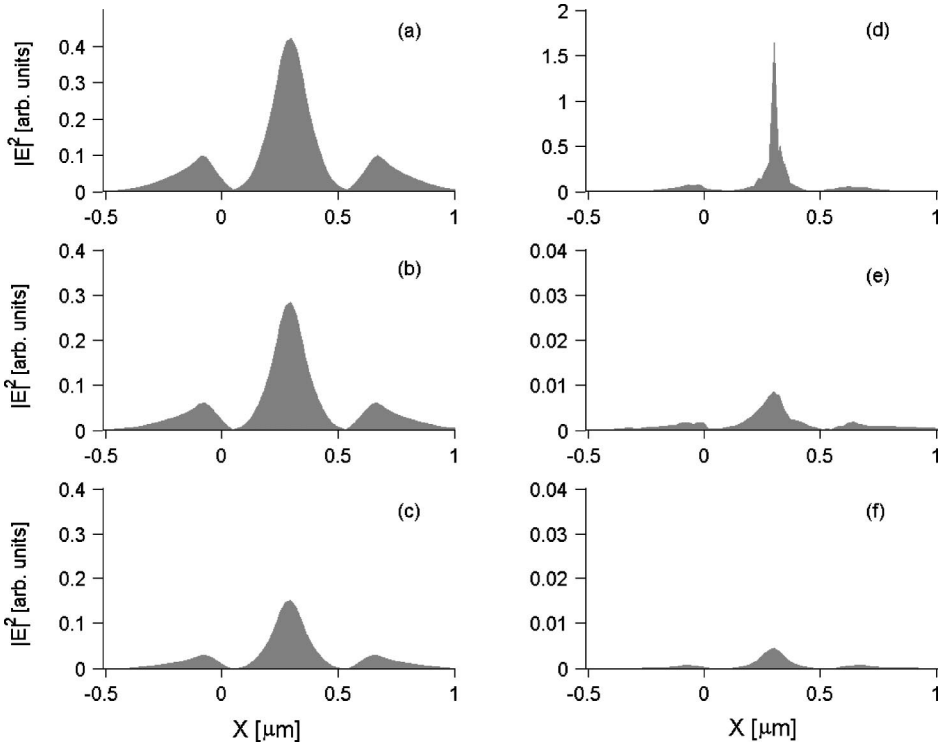

FIG. 5. The field intensity near the defect line at three different propagation times: the first row corresponds to $ct_1=32.7$ μm, the second to $ct_2=98.3$ μm, and the third to $ct_3=196.6$ μm. The graphs in the left column are for an input power of $P_{in}=1$ W/μm while the graphs on the right column are for $P_{in}=10$ W/μm. $n_2=0.2$ μm^2/W for both cases.

which is $\Delta n=2.0$, so it explains the reduction in the intensity of the transmitted pulse observed in these figures.

To study the behavior of the crystal systematically, we repeated the computations for a range of launch powers and Kerr coefficients; the resulting transmitted powers are plotted in Fig. 6. The transmitted power, in each case, was found by integrating the PSD over the frequencies near ω_0, and was then normalized to the power in the fundamental at the input.

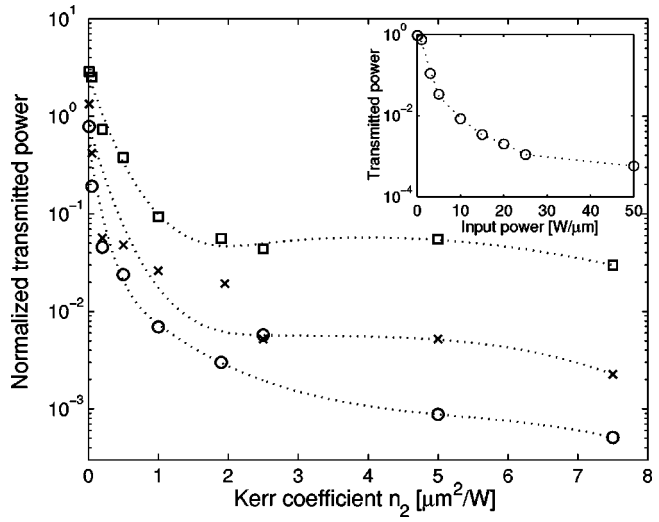

FIG. 6. The ratio of the power in the guiding mode to the input power at ω_0 vs the Kerr coefficient n_2 for three different launch powers: $P_{in}=1$ W/μm ($\square$), $P_{in}=3$ W/μm ($\times$), and $P_{in}=5$ W/μm ($\bigcirc$). The dotted lines are a guide to the eye. The inset shows a plot of the normalized transmitted power vs the input power for $n_2=0.2$ μm^2/W.

The inset in Fig. 6 contains a plot of the normalized transmitted power vs the input power for $n_2=0.2$ μm^2/W, a typical value, for example, in GaAlAs semiconductors; the plot shows a marked decrease in the normalized transmitted power with increasing input powers. For instance, the normalized transmitted power decreases by about three orders of magnitude when the input power is increased from 1 to 25 W/μm. For a crystal with a thickness of 1 μm and the same input pulse shape as in Sec. III, this corresponds to a switching energy of about 350 fJ. This demonstrates that small changes in the input power can induce large variations of the transmitted power.

Furthermore, the guided power strongly depends on the nonlinear refractive index. In fact, we observed that for large values of the Kerr coefficient n_2, the energy launched into the crystal remains confined at the first few defect rods. The fields at each of these defect sites resemble a localized pointlike defect mode. Figure 6 shows that the transmitted power, for an input power of 5 W/μm, is reduced by three orders of magnitude as compared to that at the input, if the Kerr coefficient is $n_2=7.5$ μm^2/W. At high Kerr coefficients, a saturationlike behavior is observed, with the transmitted power remaining essentially unchanged with a further increase in the Kerr coefficient. Note that for $P_{in}=1$ W/μm the saturation of the transmitted power occurs at a value of the Kerr coefficient $n_2\approx 1.5$ μm^2/W, a value that corresponds to induced changes in the refractive index $\Delta n\approx 1.5$, that is, close to Δn_{cr}. Moreover, as the Kerr coefficient increases, another phenomenon is observed, namely, the propagating field becomes highly confined at the defect rods. In fact, the overlap between the fields at neighboring rods decreases and each defect rod tends to behave as a point defect. Consequently,

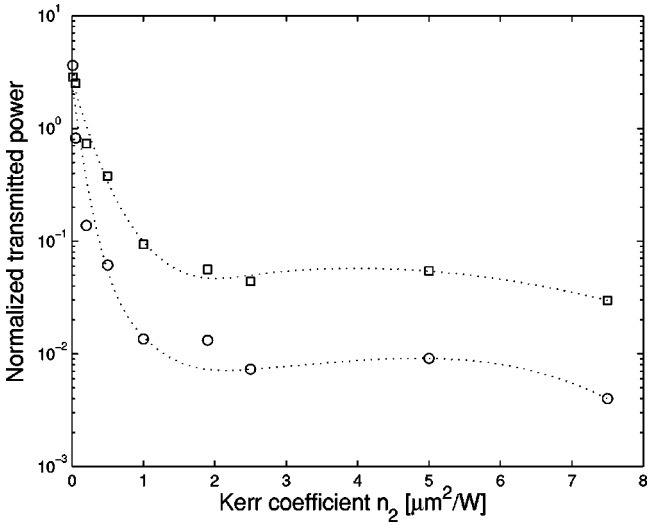

FIG. 7. The ratio of the power in the guiding mode to the input power at ω_0 vs the Kerr coefficient n_2 for two different values of the pulse spectral width: $\Delta\omega_p = 6.3\times10^{13}$ Hz (□) and $\Delta\omega = \Delta\omega_p/3 = 2.1\times10^{13}$Hz (○). In both cases, $P_{in} = 1$ W/μm.

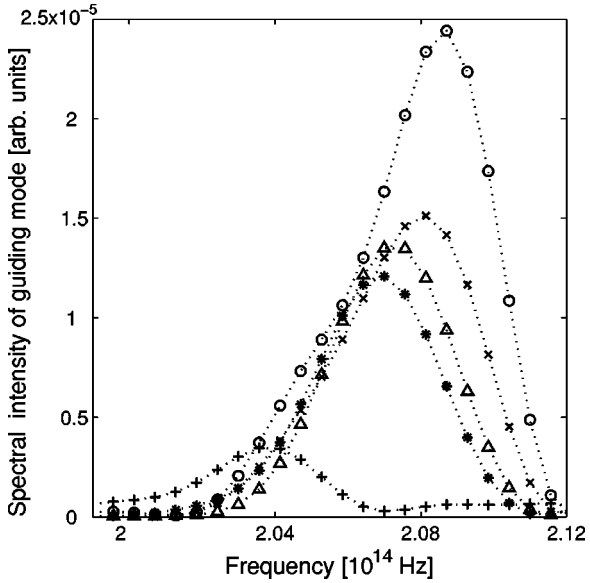

FIG. 8. The PSD of the guiding mode at the crystal output vs frequency for five different Kerr coefficients: $n_2 = 0.5$ μm^2/W (○), $n_2 = 1$ μm^2/W (×), $n_2 = 1.9$ μm^2/W (Δ), $n_2 = 2.5$ μm^2/W (*), and $n_2 = 5$ μm^2/W (+). The input power was $P_{in} = 1$ W/μm. The dotted lines are a guide to the eye.

based on an analogy with the tight binding model in solid state physics, the transmitted power in such a case will be reduced. Thus, above a nonlinearity of $n_2 \approx 3.5$ μm^2/W, for all three input powers, the transmitted power does not change significantly with any further increase in the Kerr coefficient and, apparently, saturates.

We mention that, for pulses with smaller bandwidths, steeper switching curves are observed. This phenomenon is illustrated in Fig. 7, which shows the switching curves that correspond to two pulses with different bandwidths but with the same input power. As seen in Fig. 7, the switching curve that corresponds to the pulse with a smaller bandwidth is steeper than the one that corresponds to a pulse with a larger bandwidth. This result is a consequence of the fact that, in order to switch a pulse with a smaller bandwidth, one requires a smaller shift in the frequency of the guiding mode band, and, consequently, a smaller change in the refractive index. Furthermore, Fig. 7 shows that for pulses with the same input power, the transmitted power decreases with decreasing bandwidth of the pulse. This phenomenon can be understood by noting that the transmitted power decreases with decreasing overlap between the bandwidth of the pulse and the spectral width of the mode. Thus, for a given frequency shift of the mode, this spectral overlap will be smaller for pulses with smaller bandwidths.

The frequencies of the guiding mode band can also be controlled via the change in either input power or n_2. We examined this effect in detail by calculating the PSD of the guided mode at different Kerr coefficients; the results are plotted in Fig. 8. The calculation was made for a fixed input power of 1 W/μm. The figure shows that as the nonlinear shift in the refractive index, Δn, varies, i.e., n_2 increases at a fixed input power, the peak frequency of the guided mode at the end of the crystal decreases; alternatively, the same behavior is obtained if the input power is varied. Importantly, the mode frequency shift is induced by the transmitted power and not by the input power. This can be readily seen in Fig. 8. Thus, by using the data presented in Fig. 6, one can estimate that the change in refractive index that leads to the frequency shift displayed by the curves corresponding to $n_2 = 0.5$ μm^2/W and $n_2 = 5$ μm^2/W in Fig. 8 is $\Delta n \approx 0.1$. On the other hand, numerical calculations of the band structure show that in order to obtain the same frequency shift of the guiding mode band one has to increase the refractive index by $\Delta n \approx 0.07$, that is, in agreement with the above estimate. In contrast, had we used the input power to calculate the change in the refractive index, we would have obtained $\Delta n \approx 1$. Therefore, while the *input power* changes the band structure at the input facet of the crystal, leading to strong variations in the amount of power coupled into the crystal, the spectral properties of the transmitted pulse are determined by the influence of the *transmitted power* on the guiding mode. The shift in the frequency of the guiding mode band, as n_2 is increased from 0.5 to 5.0 μm^2/W, corresponds to a wavelength shift of $\Delta\lambda \approx 40$ nm in the peak of the output spectrum.

These results show that significant frequency shifts can be achieved at reasonable input powers using the defect bandwidth of the crystal efficiently. Since the defect mode is broad, this effect can be used to ''tune'' short pulses. For example, in the case considered here, the width of the defect mode is ~ 6 THz, thus allowing a significant frequency shift across the transform limited bandwidth of a 0.15 ps pulse.

The detailed frequency shifting behavior of the defect mode can be examined by studying propagation through a shorter crystal. To do this, we propagated pulses of different powers in a crystal containing only seven rows. As explained

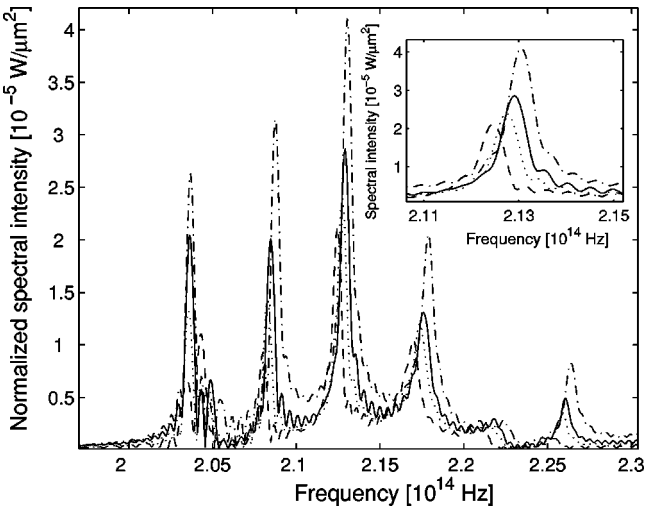

FIG. 9. The PSD of the optical field after propagating through a crystal, containing seven rows, for four different input powers: $P_{in}=3$ W/μm (dash-dot), $P_{in}=7$ W/μm (solid), $P_{in}=10$ W/μm (dot), and $P_{in}=15$ W/μm (dash). The inset plots the calculated PSD, around the central spectral peak. The Kerr coefficient was $n_2=0.2$ μm^2/W.

in Sec. II, the defect mode of a shorter crystal is composed of well resolved spectral peaks. This structure is seen clearly in Fig. 9, which shows the transmitted spectra of the crystal at four different input powers, for $n_2=0.2$ μm^2/W. The calculations were also repeated for crystals with a larger number of defects and the PSD of the corresponding output pulses displayed a greater number of more closely spaced peaks. The peaks become narrower on increasing the number of defects and those at higher frequencies are suppressed so that the overall bandwidth of the mode is reduced.

Figure 9 also shows the shift in the frequency of the defect mode band with varying input powers. The frequency shift of the peaks has an approximately linear dependence on the input power and is almost the same for each peak. Thus, each increase of 5 W/μm in the input power induces a frequency shift of $\sim$0.3 THz in the central peak. Another characteristic of the PSD in Fig. 9 is that, as the input power increases, the relative power distribution among the peaks changes. This behavior is also at the origin of the overall downward shift in the PSD shown in Fig. 8. Notice that in the case shown in Fig. 8, the PSD corresponds to a longer crystal so that the fine structure of the mode spectra is not resolved. Furthermore, as the power increases, the width, in frequency, of each peak decreases; we attribute this behavior to the fact that as the power increases the light becomes more confined at the defect rods, so that there is less energy loss in the transverse direction. However, we are presently investigating this phenomenon in more detail. Moreover, note that the narrow peaks of 0.5 THz, seen in these small crystals, could be used, for instance, in a WDM transmission system. For example, the frequency shift of 0.3 THz, for a 5 W/μm increase in the input power, corresponds to a span of about three channels, in a 10 Gigabits WDM transmission line with an interchannel separation of 0.8 nm.

As a final remark, we point out that the line defects investigated here can be incorporated into more complex integrated optoelectronic devices. For instance, one can take advantage of the nonlinear phase shifts induced by line defects and use them for one arm in a Mach-Zehnder interferometer [28] or as the active region of a Fabry-Pérot resonator. The advantage of using a line defect instead of a CROW (as suggested in Ref. [28]) is that this choice can lead to larger nonlinear phase shifts per unit length and, therefore, to more compact devices.

V. CONCLUSIONS

In this article we have demonstrated the effects produced by 1D defects made from a material with Kerr-type nonlinearities, which are embedded in a 2D PC. We have demonstrated that, by achieving a strong confinement of the guiding mode in the defect line, one enhances the efficiency of the third-harmonic generation process. The characteristics of this process and its dependence on the parameters of the defect rods have been discussed and explained. All numerical simulations have been performed starting from the complete Maxwell's equations, thus avoiding common approximations that are made when one investigates the propagation of waves in nonlinear media. Also, we have discussed the implications of our results to the design of integrated all-optical devices, namely, frequency selectors and third-harmonic generators.

We have also demonstrated that, due to the nonlinear response of Kerr material embedded into the 2D PC, the transmitted power in the defect line is strongly dependent on the input power. This phenomenon can be used in all-optical devices. These results could also be extended to materials with $\chi^{(2)}$ nonlinearities. Higher efficiencies for second-harmonic and TH generation (using sum frequency generation) are expected in similar structures with 1D $\chi^{(2)}$ defects in a linear 2D PC due to the highly enhanced fields.

Finally, we mention that the phenomena discussed here can be translated to photonic crystal fibers (PCFs), consisting of a periodic lattice of air holes that run along an optical fiber. Thus, by incorporating nonlinear materials in such devices, one can take advantage of the strongly confined modes supported by the PCF. This strong localization enhances the nonlinear behavior of these modes, an effect that can have important technological applications.

ACKNOWLEDGMENTS

The authors thank Hongling Rao, R. Scarmozzino, T. Izuhara, and F. Pizzuto for many useful discussions on the FDTD method. This work has been supported by the NIST Advanced Technology Program Cooperative Agreement No. 70NANB8H4018 and also in part by a DARPA Optocenter: BROWNU-1119-24596.

[1] E. Yablonovitch, Phys. Rev. Lett. **58**, 2059 (1987).
[2] S. John, Phys. Rev. Lett. **58**, 2486 (1987).
[3] E. Yablonovitch and T. J. Gmitter, Phys. Rev. Lett. **63**, 1950 (1989).
[4] R. D. Meade, A. Devenyi, J. D. Joannopoulos, O. L. Alerhand, D. A. Smith, and K. Kash, J. Appl. Phys. **75**, 4753 (1994).
[5] A. Mekis, J. C. Chen, I. Kurland, S. Fan, P. R. Villeneuve, and J. D. Joannopoulos, Phys. Rev. Lett. **77**, 3787 (1996); A. Mekis, S. Fan, and J. D. Joannopoulos, Phys. Rev. B **58**, 4809 (1998).
[6] S. Y. Lin, E. Chow, V. Hietala, P. R. Villeneuve, and J. D. Joannopoulos, Science **282**, 274 (1998).
[7] S. Fan, P. R. Villeneuve, J. D. Joannopoulos, and H. A. Haus, Phys. Rev. Lett. **80**, 960 (1998); S. Fan, P. R. Villeneuve, J. D. Joannopoulos, M. J. Khan, C. Manolatou, and H. A. Haus, Phys. Rev. B **59**, 15882 (1999).
[8] M. J. Steel, M. Levy, and R. M. Osgood, IEEE Photonics Technol. Lett. **12**, 1171 (2000).
[9] M. J. Steel, M. Levy, and R. M. Osgood, J. Lightwave Technol. **18**, 1289 (2000); **18**, 1297 (2000).
[10] J. P. Dowling, M. Scalora, M. J. Bloemer, and C. M. Bowden, J. Appl. Phys. **75**, 1896 (1994).
[11] S. G. Johnson, C. Manolatou, S. Fan, P. R. Villeneuve, J. D. Joannopoulos, and H. A. Haus, Opt. Lett. **23**, 1855 (1998).
[12] B. D'Urso, O. Painter, J. O'Brian, T. Tombrello, A. Yariv, and A. Scherer, J. Opt. Soc. Am. B **15**, 1155 (1998); O. Painter, J. Vuckovic, and A. Scherer, *ibid.* **16**, 275 (1999).
[13] P. Halevi and F. R. Mendieta, Phys. Rev. Lett. **85**, 1875 (2000).
[14] A. Figotin, Y. A. Godin, and I. Vitebsky, Phys. Rev. B **57**, 2841 (1998).
[15] P. R. Villeneuve, D. S. Abrams, S. Fan, and J. D. Joannopoulos, Opt. Lett. **21**, 2017 (1996).
[16] T. V. Dolgova, A. I. Maidykovski, M. G. Martemyanov, A. A. Fedyanin, and O. A. Aktsipetrov, JETP Lett. **75**, 15 (2002).
[17] M. Scalora, J. P. Dowling, C. M. Bowden, and M. J. Bloemer, Phys. Rev. Lett. **73**, 1368 (1994).
[18] S. John and N. Akozbek, Phys. Rev. Lett. **71**, 1168 (1993).
[19] A. R. McGurn, Phys. Lett. A **251**, 322 (1999); **260**, 314 (1999).
[20] S. F. Mingaleev and Y. S. Kivshar, Phys. Rev. Lett. **86**, 5474 (2001); S. F. Mingaleev, Y. S. Kivshar, and R. A. Sammut, Phys. Rev. E **62**, 5777 (2000).
[21] K. S. Yee, IEEE Trans. Antennas Propag. **14**, 302 (1966).
[22] A. Taflove and S. C. Hagness, *Computational Electrodynamics: The Finite-Difference Time-Domain Method* (Artech House, Boston, 2000).
[23] RSoft Design Group, http://www.rsoftdesign.com
[24] M. Koshiba, Y. Tsuji, and S. Sasaki, IEEE Microwave Guid. Wave Lett. **11**, 152 (2001).
[25] S. F. Mingaleev and Y. S. Kivshar, Opt. Lett. **27**, 231 (2002); J. Opt. Soc. Am. B **19**, 2241 (2002).
[26] A. Yariv, Y. Xu, R. K. Lee, and A. Scherer, Opt. Lett. **24**, 711 (1999); Y. Xu, R. K. Lee, and A. Scherer, J. Opt. Soc. Am. B **17**, 387 (2000).
[27] A. L. Reynolds, U. Peschel, F. Lederer, P. J. Roberts, T. F. Krauss, and P. J. L. de Maagt, IEEE Trans. Microwave Theory Tech. **49**, 1860 (2001); U. Peschel, A. L. Reynolds, B. Arredondo, F. Lederer, P. J. Roberts, T. F. Krauss, and P. J. L. de Maagt, IEEE J. Quantum Electron. **38**, 830 (2002).
[28] M. Soljacic, S. G. Johnson, S. Fan, M. Ibanescu, E. Ippen, and J. D. Joannopoulos, J. Opt. Soc. Am. B **19**, 2052 (2002).